J Electroceram (2011) 27:189–196
DOI 10.1007/s10832-011-9664-5

Structural and mechanical properties characterization of barium strontium titanate (BST) ceramics

M. H. Badr · L. M. Sharaf El-Deen · A. H. Khafagy · D. U. Nassar

Received: 10 April 2011 / Accepted: 7 November 2011 / Published online: 22 November 2011

Abstract $Ba_{(1-x)}Sr_{(x)}TiO_3$ ceramics, where x=0.05, 0.10, 0.15, and 0.20, were prepared by solid state reaction technique. X-ray diffraction analysis confirmed the formation of single phase perovskite structures. Mechanical properties such as ultrasonic attenuation, longitudinal wave velocity, and longitudinal elastic modulus were studied by an ultrasonic pulse echo technique at 2 MHz. Investigations of ceramic microstructures and mechanical properties showed its dependence on composition and sintering time. Increasing of Sr content, x, resulted in a decrease in bulk density and ultrasonic attenuation and an increase in velocity and modulus. Also, size of crystallites and c/a ratio were found to decrease with increasing of x, and increased with increasing of sintering time. High temperature ultrasonic studies showed, in addition to Curie phase transition, two relaxation peaks and its origin was investigated. The acquired structural and mechanical results were correlated and discussed.

Keywords BST ceramics · Phase transition · Ultrasonic attenuation · Longitudinal velocity · Longitudinal elastic modulus · XRD

1 Introduction

Barium strontium titanate (BST) ceramics, $Ba_{(1-x)}Sr_{(x)}TiO_3$, are solid solutions composed of barium titanate and strontium titanate. These ceramics have high electronic interests due to its high dielectric constant, alterable Curie temperature, low dielectric loss, and high tunability of dielectric behaviour. Because of its favorable pyroelectric, ferroelectric, and piezoelectric characteristics, BST materials have been widely used in preparation of dielectric capacitors, positive temperature coefficient resistors (PTC), transducers, piezoelectric sensors, dynamic random access memories (DRAM), microwave phase shifters, and uncooled infrared detectors [1–10].

BST ceramics have been prepared by the conventional calcining of mixed powders of oxides or carbonates. The main drawback of this technique is the repeated process of heat treatment and grinding that may cause contamination. However, it is more preferred for its wide availability and economical use of large batch processing than other reported methods, e.g., sol–gel [11–14], co-precipitation [15], hydrothermal [16, 17], polymeric precursor [18], and other methods that required expensive inorganic or organic chemicals as the starting materials [19, 20].

An elastic modulus anomaly and a mechanical loss peak were reported in pure barium titanate, $BaTiO_3$, materials at three phase transitions [21, 22]. Namely, rhombic to orthorhombic (−100 to –80°C), orthorhombic to tetragonal (0 to 5°C) and tetragonal to cubic or ferroelectric to paraelectric (~130°C). Also, some mechanical losses, due to relaxation processes, have been observed in materials having coarse grains in the ferroelectric phase and were attributed to the interaction between domain walls and diffusion of oxygen vacancies.

Isovalent dopants, such as strontium or lead, have been employed to lower or raise the Curie point for particular microwave applications such as phase shifters, tunable filters, delay lines, and tunable oscillators [23–26]. Using niobium oxide in few percent, in the system $Ba(Ti,Nb)O_3$, caused a severe decrease in Curie temperature and raised

M. H. Badr · L. M. S. El-Deen · A. H. Khafagy (✉) · D. U. Nassar
Faculty of Science, Physics Department, Minufiya University, Shebin El-Kom, Minufiya 32511, Egypt
e-mail: khafagy47@yahoo.com

the tetragonal-orthorhombic and orthorhombic–rhombic transition points. To control porosity, MgO and MnO_2 dopants (1 wt.% each) were added to $Ba_{(1-x)}Sr_{(x)}TiO_3$ ceramics (x=0.25, 0.50, 0.75, 0.90) sintered at 1260°C [27].

Most of the reported dielectric studies on $Ba_{(x)}Sr_{(1-x)}TiO_3$ ceramics in the frequency range 1–1000 KHz aimed to investigate the dependence of phase transition on composition. A linear dependence of Curie temperature, T_c, on the stoichiometric percentage of Ba, x, in the form: $T_c(°C) = -195.0 + 322.2x$, has been reported [28]. On the other hand and to our knowledge, mechanical investigations are scarce and limited to some published work dealt with mechanical losses (internal frictions) and shear moduli of $Ba_{(x)}Sr_{(1-x)}TiO_3$ (x=0.4, 0.55, 0.7, 0.8) at the low frequency range 0.1–1 Hz with an inverted pendulum [21–23, 29].

This work aims to understand thoroughly the effects of sintering conditions and composition on the structure and mechanical properties (such as elastic modulus, attenuation, and velocity of ultrasonic waves) of $Ba_{(1-x)}Sr_{(x)}TiO_3$ ceramics (with x=0.05,0.1,0.15 and 0.2), sintered at 1250°C for 2, 4, 8, and 10 h. X-ray diffraction and ultrasonic techniques (at a frequency of 2 MHz) were used to characterize the structure and phase transitions of the prepared BST ceramics.

2 Experimental

BST ceramics with the chemical formula $Ba_{(1-x)}Sr_{(x)}TiO_3$, where x=0.05, 0.1, 0.15, and 0.2, were prepared by the conventional solid state reaction technique. Reagent-grade $BaCO_3$, $SrCO_3$, and TiO_2 were mixed in the appropriate molar ratios and ground thoroughly by an agate vibratory micro mill for 6 h. The mixtures were calcined at 1100°C for 11 h in alumina crucibles opened to air. The obtained calcined compositions were ground for another 8 h. The produced fine powders were pressed into disc-shaped pellets (10 mm in diameter and 0.6–1.5 mm in thickness) at an isostatic pressure of 6 t. The pelletized samples were finally sintered at 1250°C for 2, 4, 8, and 10 h. The density of ceramics was measured by the conventional Archimedean method. X-ray diffraction (XRD) patterns were recorded with Bruker AXS X-ray diffractometer (D8 Advance) using Cu Kα radiation.

Attenuation of ultrasonic waves and longitudinal velocity of wave propagation were determined by employing the conventional pulse-echo technique at room temperature and during heating. In this technique, commercial x-cut quartz crystals actuated by an ultrasonic flaw detector (KrautKramer USM-2) were used for transmitting and receiving the generated 2 MHz longitudinal ultrasonic waves. The waves were coupled to the tested sample by silicon grease. The received echoes, from the back end of a sample, were characterized by its equal-distance and exponentially decayed patterns of electrical signals displayed on the ultrasonic flaw detector screen. To measure ultrasonic attenuation (α), the heights of some successive echoes were used according to this equation [30]:

$$\alpha = [-20\log(A_m/A_n)]/2(m-n)\,d.$$

Where, A_m and A_n are the amplitudes of the m^{th} and n^{th} echoes and d is the specimen thickness. The calculated values of α for the tested ceramics were accurate to ±0.1% db/mm. Also, values of longitudinal ultrasonic wave velocities (V_L=2 d/t) and longitudinal elastic moduli ($L=\rho V_L^2$) were calculated by using the transient time (t) of flight between successive echoes.

3 Results

Average values of bulk densities, of prepared $Ba_{(1-x)}Sr_{(x)}TiO_3$ ceramics sintered at 1250ºC for 2, 4, 8, and 10 h, are listed in Table 1. The listed values reveal the dependence of density on strontium content and sintering time. It is observed that the density of samples decreases as the Sr content, $0.05 \le x \le 0.2$, increases for each sintering time. Furthermore, the density values are increased as the time of sintering is increased, for each Sr content.

Figure 1 shows the dependence of ultrasonic attenuation (α), measured at room temperature, on the composition of $Ba_{(1-x)}$ $Sr_{(x)}TiO_3$ ceramics sintered at 1250°C for different times. Inspection of this figure reveals that α is dependent on the composition, i.e., it is linearly decreased at different rates with the increase of x, as indicated by regression lines. On the other hand, Fig. 2 shows the effect of sintering time, at a sintering temperature of 1250°C, on the attenuation of ultrasonic waves. It is observed that, the highest values of α are at the lowest sintering time, 2 h, and a rapid decrease is noticed up to 4 h. Then, a slow and linear (R^2=1.00, 1.00, and 0.99 for sintering times of 4, 8, and 10 h, respectively) decrease is detected up to the final investigated sintering time, 10 h. It is worth mentioning that, the absolute values of these slopes, Fig. 2, increase as the Sr content, x, increases according to the equation: $y = 0.13\ln(x) - 0.89\left(R^2 = 1.000\right)$, where y is α (db/cm) per sintering time (h).

Figure 3 shows the dependence of longitudinal ultrasonic velocity, V_L, on Sr content, x, of $Ba_{(1-x)}Sr_{(x)}TiO_3$ ceramics sintered at 1250°C for different times. The observed results shows a linear increase in V_L with the increase of x for all sintering times. However, the effect of sintering time on V_L reveals a quadratic behavior for all compositions, see Fig. 4. A rapid increase in longitudinal velocity is

Table 1 Density, ultrasonic attenuation, longitudinal velocity and longitudinal elastic modulus of $Ba_{(1-x)}Sr_xTiO_3$ ceramics

Sr content, x	Sint. time at 1250°C (h)	Density, ρ (kg/m^3)	Ultrasonic atten., α (dB/cm)	Long. Velocity, V_L (m/s)	Long. Elastic Modulus, L (GPa)
0.05	2	4450	21	683.6	2.1
	4	4780	10	1293.3	8.1
	8	5220	8	1355.2	9.58
	10	5400	7	882.1	4.2
0.10	2	4100	19	813.1	2.7
	4	4433	9.5	1397.6	8.7
	8	4713	7	1454.4	9.97
	10	5000	6	1034.6	5.35
0.15	2	3850	16	1120.5	4.83
	4	4200	8	1456.8	8.9
	8	4400	6	1610.5	11.4
	10	4880	4	1283.8	7.9
0.20	2	3710	13	1269.3	5.98
	4	3850	7	1573.0	9.53
	8	4000	4	1697.6	11.52
	10	4740	3	1352.8	8.67

observed with increasing time from 2 h to 4 h, followed by a slower increase up to 8 h, and then decreases until 10 h. The longitudinal elastic modulus, L, shows same trends of composition and sintering time dependences as those of V_L (see Table 1).

X-ray diffraction (XRD) patterns for prepared $Ba_{(1-x)}Sr_{(x)}TiO_3$ ceramics sintered at 1250°C for 2 h are shown in Fig. 5. All XRD results obtained for all tested BST ceramics are listed in Table 2, for brevity. The results in Fig. 5, recorded at room temperature, show all major XRD peaks for each tested sample. This confirms the formation of a single phase perovskite BST structure. All peaks are indexed corresponding to its reflections of different polycrystalline orientations [28, 33, 35] as indicated with (110) index as the high intensity major peak.

Figure 6 Shows variations of the ultrasonic attenuation, α, with temperature for x=0.05 and 0.2, sintered at 1250°C for 2 h. This figure reveals a well-defined damping peaks at 320 and 285°C for x=0.05 and 0.2, respectively. Also, a big

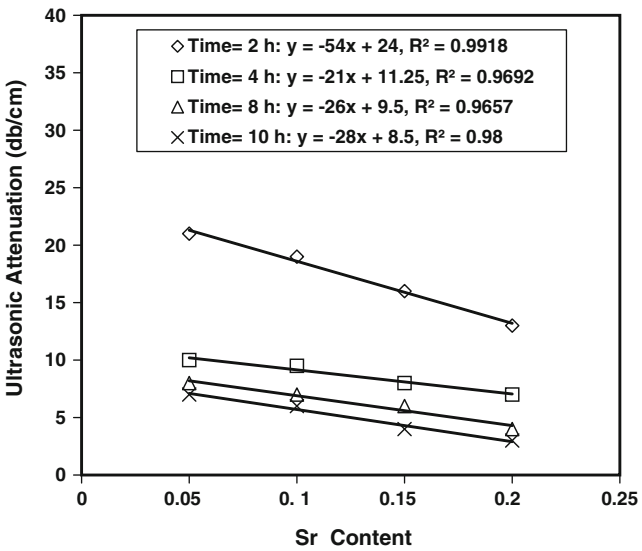

Fig. 1 Variations of ultrasonic attenuation with strontium content of $Ba_{(1-x)}Sr_{(x)}TiO_3$ ceramics, sintered at 1250°C for different times

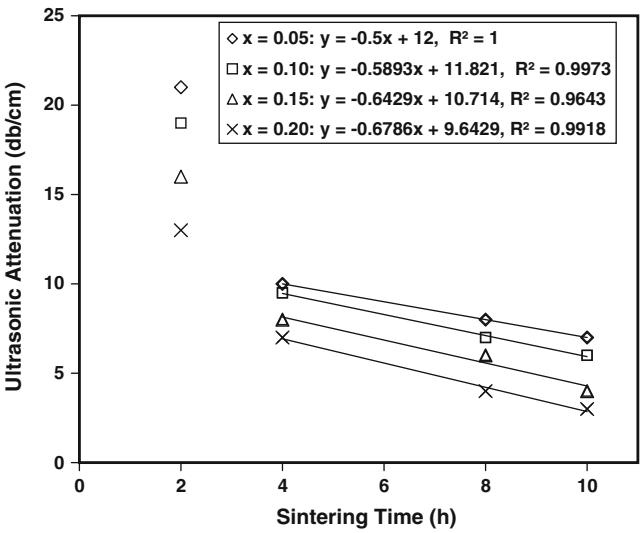

Fig. 2 Variations of ultrasonic attenuation with sintering time of $Ba_{(1-x)}Sr_{(x)}TiO_3$ ceramics, where x=0.05, 0.1, 0.15, and 0.2

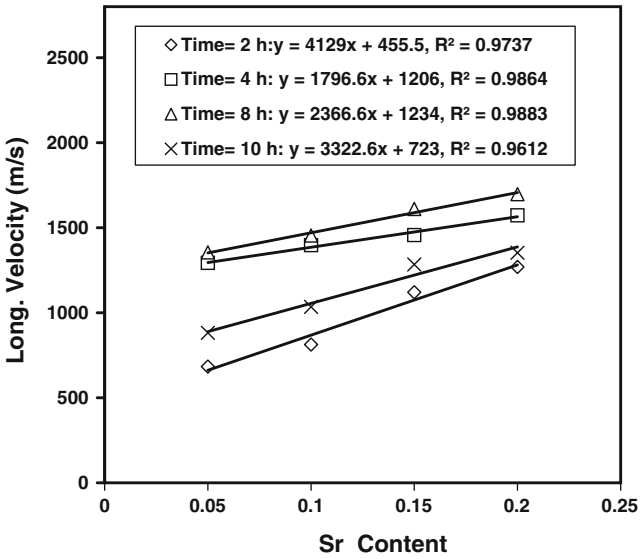

Fig. 3 Variations of longitudinal velocity with Sr content of $Ba_{(1-x)}Sr_{(x)}TiO_3$ ceramics, sintered at 1250°C for different times

shoulder for each ceramic was observed near 0°C temperature. Moreover, another two small damping peaks are occurred for both specimens below the high temperature damping peaks. The first peak occurs at 183°C for both ceramics, whereas the second peak is observed at 268°C for x=0.05 and at 242°C for x=0.2.

4 Discussion

4.1 Density

Variations of bulk density of $Ba_{(1-x)}Sr_{(x)}TiO_3$ ceramics, where 0.25≤x≤0.9, have been investigated [31, 32]. The reported results showed that the measured density (gm/cm^3)

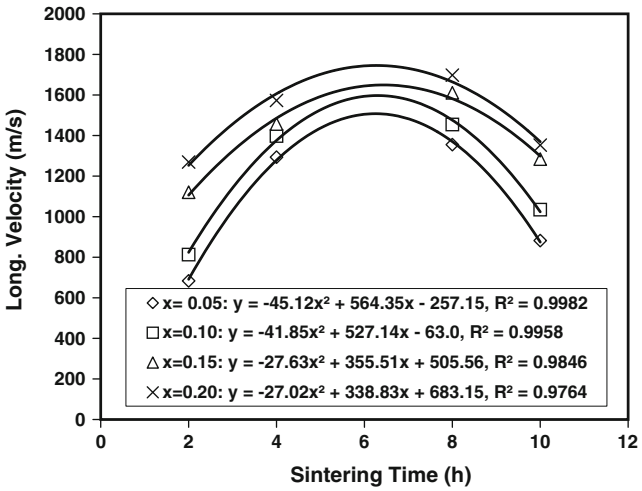

Fig. 4 Variations of the longitudinal velocity with the sintering time of $Ba_{(1-x)}Sr_{(x)}TiO_3$ ceramics, where x=0.05, 0.1, 0.15, and 0.2

of the doped and undoped BST samples with 0.25≤x≤0.75, sintered at 2230 and 2260°C, could be reasonably fitted by the equation: $\rho(x) = 5.42 - 1.88x$. This equation showed a linear decrease in density from 4.95 to 4.01 (gm/cm^3) with increasing of Sr content from x=0.25 to x=0.75. In the present work, a lower range, 0.05≤x≤0.2, of Sr content is investigated and the average density values are illustrated in Table 1. The measured Archimedean density shows a decrease from 4,450 to 3,710 kg/m^3 as x is increased from 0.05 to 0.2, for samples sintered at 1250°C for 2 h (see Table 1 for other sintering times). This is in agreement, within experimental error, with the highest range of Sr content of the previously mentioned results [31, 32]. The observed decrease in density of our samples is attributed to the increased porosity associated with increasing of Sr content [32], as well as, the fact that the atomic weight of Sr (87.62) is lower than that of Ba (137.3).

Dependences of bulk density of BST ceramics on sintering temperature [31, 32] and on sintering temperature and soaking time [33] were investigated. Reported results [31, 32] showed that density was increased for sintering temperatures in the range from 1200 to 1230°C, and maintained constant beyond 1230°C up to 1260°C. Also, an increase in density was observed [33] as sintering time was increased from 2 h to 4 h for soaked pellets sintered at the same temperature. Furthermore, densities were increased from 5.62 to 5.68 (gm/cm$^{3)}$ when sintering temperature was increased from 1330 to 1350°C, respectively, for samples sintered for 6 h. This suggests that high density BST ceramics could be produced by reaction sintering process. Let us now return to Table 1 to examine the dependence of density of our BST ceramics on sintering time. As can be seen, a similar behavior, to that of Ref. [33], has been obtained for all tested specimens where ρ is increased for each composition with increasing of sintering time from 2 to 10 h. Therefore, the increase in density with the increase of sintering time in the range 2–10 h could be attributed to shrinkage in these ceramics [33, 34].

4.2 XRD analysis

Effects of composition and sintering time on crystallinity of tested BST ceramics are investigated, and XRD patterns are illustrated in Fig. 5. The lattice parameters for the polycrystalline tetragonal phase were calculated from the interplannar, d_{hkl}, distance values and the provided x-rays cards. The ratio (c/a) was determined and typical values are shown in Table 2. The dependence of (c/a) on Sr content reveals its decrease, in general, as Sr content is increased; the tetragonal phase approaches the cubic one. On the other hand, it is also observed that (c/a) increases with increasing of sintering time from 2 h up to 4 h and maintained constant over all investigated range up to

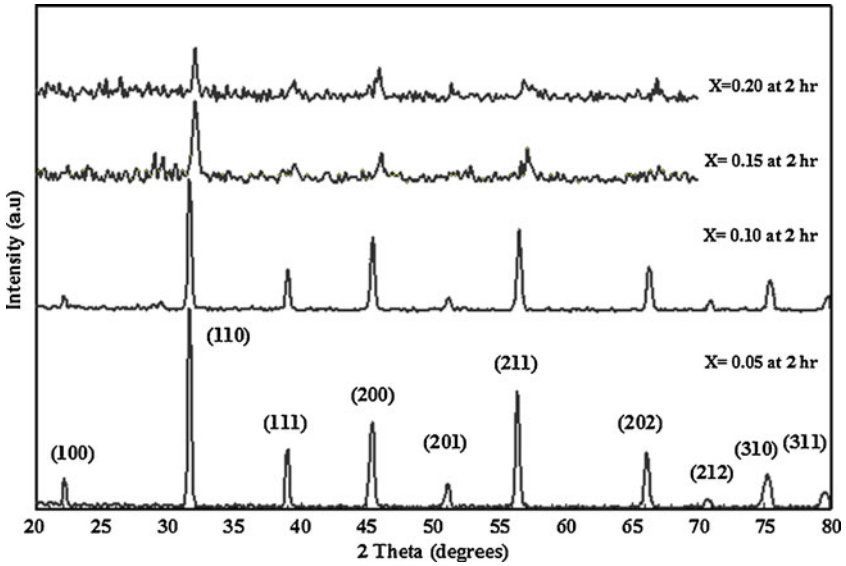

Fig. 5 XRD records of $Ba_{(1-x)}Sr_{(x)}TiO_3$ ceramics, where x=0.05, 0.1, 0.15, and 0.2, sintered at 1250°C for 2 h

10 h. The average crystallite diameter, D_{hkl}, is evaluated in terms of x-ray line broadening using the Scherrer's equation: $D_{hkl} = k\lambda/\beta \cos\theta$, where λ is the x-ray wavelength (λ=5418 Å), β is line width at half maximum (FWHM), θ is Bragg angle, and k=0.9. The average values of D_{hkl}, listed in Table 2, provide another confirmatory evidence of the previously mentioned effect of increasing Sr content, i.e., the particle size is decreased with Sr content and increased with sintering time.

It has been well known that crystallinity of BST ceramics is improved by increasing of calcining or sintering temperature. Referring to the reported XRD data on BST ceramics [28, 34], lattice parameters were found to increase with increasing of calcining temperatures from 1200 to 1400°C for each Sr content. Also, an increase in Sr content was accompanied by a decrease in lattice parameters and particle size, was reported as well. Two interpretations were proposed [34], firstly, at low calcining temperatures the powders existed in a more strained form with the atomic entities in nonequilibrium positions which relaxed to equilibrium at higher temperatures, and thus lattice parameter were increased. Secondly, domain mobility

Table 2 Lattice parameters, a, c, the ratio (c/a), and the particle size of $Ba_{(1-x)}Sr_xTiO_3$ ceramics

Sr content, x	Sint. time at 1250°C (h)	Lattice parameter a (Angestrom)	Lattice parameter c (Angestrom)	c/a ratio	Particle size, D_{hkl} [Sherrer's Eqn.] (nm)
0.05	2	3.9771	3.9883	1.0028	31.5050
	4	3.9820	4.0170	1.0088	34.3585
	8	3.9820	4.0170	1.0088	36.0049
	10	3.9820	4.0170	1.0088	36.4174
0.10	2	3.9771	3.9883	1.0028	28.6321
	4	3.9820	4.0170	1.0088	32.9564
	8	3.9820	4.0170	1.0088	34.3786
	10	3.9820	4.0170	1.0088	35.0548
0.15	2	3.9724	3.9703	0.9995	27.0436
	4	3.9771	3.9883	1.0028	27.4528
	8	3.9771	3.9883	1.0028	28.0208
	10	3.9771	3.9883	1.0028	28.0347
0.20	2	3.9724	3.9703	0.9995	21.5120
	4	3.9471	3.9471	1.0000	23.5497
	8	3.9471	3.9471	1.0000	25.6186
	10	3.9471	3.9471	1.0000	27.4417

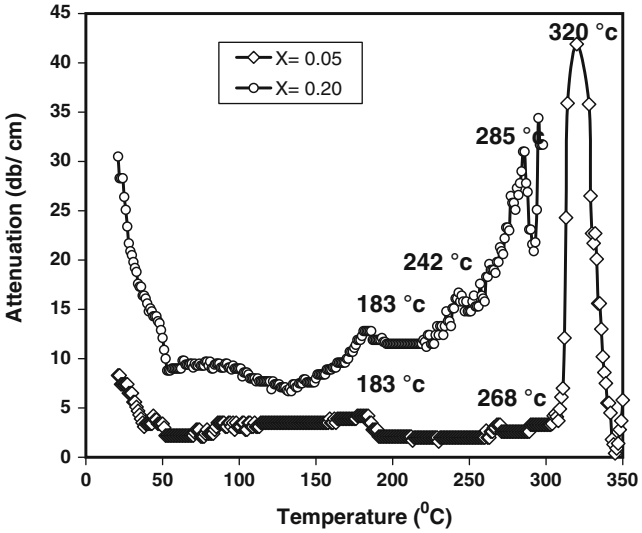

Fig. 6 Variations of ultrasonic attenuation with temperature (at 2 MHz) of $Ba_{(1-x)}Sr_{(x)}TiO_3$ ceramics for x=0.05 and 0.2, sintered at 1250°C for 2 h

was restricted at lower temperatures due to pinning of the domain boundaries by crystal defects, which became easier upon increasing of calcining temperatures, leading to an increase in the particle size. Bearing in mind, these interpretations were proposed when Ba replaced Sr in $Ba_{(x)}Sr_{(1-x)}TiO_3$ ceramics [34]. Thus, the converse action of the above assumptions will be in favor of our results on $Ba_{(1-x)}Sr_{(x)}TiO_3$ ceramics, i.e., (c/a) ratio is decreased upon increasing of Sr, at the expense of Ba, and increases with sintering time, for same Sr content, as confirmed by Scherrer's particle size results, see Table 2.

4.3 Attenuation, elastic modulus, and ultrasonic velocity

The observed decrease in density with the increase of Sr content, see Table 1, was attributed to an increase in porosity and differences in atomic weights of Sr and Ba. It has been known [36] that heterogeneities, such as pores, microcrakes, and grains, decrease the velocity of both longitudinal and shear ultrasonic waves. Also, particle size can affect ultrasonic velocity in a manner that increasing the average particle size decreases the velocity and increases the attenuation. Now, referring to our XRD results and the calculated values of lattice parameters and (c/a) ratio, Table 2, it is noted that this ratio is decreased as x is increased. Furthermore, this ratio is increased for each specimen upon increasing of sintering time, indicating that the particle size is decreased, as seen in Fig. 5, where the intensities of the diffraction peaks are decreased which is in good agreement with the reported result [34].

Microstructures of $Ba_xSr_{1-x}TiO_3$ ceramics, with x=1, 0.7, 0.6, and 0.5, were described [37], and the reported results showed an abnormal grain growth obtained with coarse grains of about 50 μm, surrounded by fine grains of about 2 μm. Also, the grain size was increased with increasing of Ba content or, in other words, substitution of Ba by Sr inhibited growth of grains. Therefore, the ceramic microstructure, by this way, has its effect on ultrasonic velocity, elastic modulus, and attenuation of ultrasonic waves as follows: increasing of Sr content would increase porosity [32], and decreases the particle sizes [34, 37] in the formed perovskite polycrystalline structures. This in turn decreases the attenuation of ultrasonic waves propagated in these ceramics, increases elastic modulus, and ultrasonic velocity [36], as obtained in Fig. 1, Table 2, and Fig. 3, respectively. On the other hand, sintering time has its effect on the microstructure of BST ceramics in the manner that it makes it denser due to shrinkage and reaction sintering process. Also, this increases velocity and modulus, as observed in Fig. 4 and Table 2, in the range 2–8 h. However, the observed decrease in velocity and modulus in the range 8–10 h is due to relaxation of the strained microstructure that occurs as the sintering time is increased. On the other hand, the attenuation is rapidly decreased in the sintering time range 2–4 h, Fig. 2, as the microstructure is more strained with its atomic entities in nonequilibrium positions, and then slowly decreased up to 10 h, final investigated sintering time, as the equilibrium of the microstructure is attained.

4.4 Temperature dependence of ultrasonic attenuation

Mechanical loss (internal friction, Q^{-1}) and shear modulus of BST ceramics, with Sr content x=0.2, 0.3, 0.45, and 0.6, were studied [29] as a function of temperature in the range from −150 to 100°C and at 0.1, 0.3, and 1 Hz operating frequencies, using a torsion pendulum. The reported results showed that the modulus curves disclosed three anomalies connected to three loss peaks p_1, p_2, and p_3 in the order of lowering temperatures. These peaks were related to three phase transitions: cubic to tetragonal (C-T, known as the Curie transition), tetragonal to orthorhombic (T-O), and orthorhombic to rhombohedral (O-R), respectively. It has also been reported [29] that the temperatures of these transitions decreased with increasing of Sr content in BST materials, and loss peaks became broad. This broadness was attributed to a core-shell structure of its microstructure that led to more diffused phase transitions with rising of Sr content. Also, internal friction investigations on BST ceramics [21, 22, 29] showed in addition to the above phase transitions, another one or two relaxation peaks that was/were observed and located below the Curie transition in the ferroelectric tetragonal phase. The origin of such relaxation peaks was interpreted according to the calculated values of its activation energy, for example, relaxation

peaks of activation energy smaller than 1.1 eV in BST systems [22, 29] could be attributed to diffusion of oxygen vacancies associated with domain walls. Whereas, relaxation peaks with energies larger than 1.1 eV were interpreted to diffusion of point defects in ferroelectric phase of these ceramics.

Although, comparison between mechanical measurements [21, 29] and other dielectric ones [37, 39] on BST materials makes it possible to show that these measurements are fully connected; there are some notations which could be summarized in the following manner: i) Dielectric measurements [39] of the real part of permittivity confirmed that the Curie temperature, of investigated BST materials, was frequency-independent in the range 0.1–200 kHz, see Fig. 8 of Ref. [39]. On the other hand, variation of dielectric loss showed some temperature anomalies, Fig. 9 [39], due to frequency variations in the above tested range. ii) Mechanical measurements, Q^{-1} versus temperature, of $Ba_{0.8}Sr_{0.2}TiO_3$ doped with 1 wt.% MgO at 0.1, 0.3, and 1 Hz operating frequencies showed Curie temperature to be frequency-independent, see Fig. 6 of Ref. [29]. iii) All previous investigations, specifically mechanical, on BST ceramics were carried out at low frequencies (several Hz) and no work has been performed in the MHz range, to the best of our knowledge. Therefore, in the present work, the temperature dependence of ultrasonic attenuation of $Ba_{(1-x)}Sr_{(x)}TiO_3$ ceramics with x=0.05 and 0.2 are investigated and carried out at 2 MHz, see Fig. 6. These results could be interpreted as follows: the high temperature attenuation peaks at 320 and 285°C for ceramics with x=0.05 and 0.2, respectively, indicate the Curie transition temperatures of these materials. However, its occurrence in this range of temperatures, due to the high operated frequency, agrees very well with previous results [22, 29] in that the peak position is lowered on the temperature scale and becomes more dispersed with the increase of Sr content. Also, the observed shoulders for both ceramics, Fig. 6, refer to the right wing of the tetragonal to orthorhombic phase transition which seems to occur around 0°C temperature. The small damping peaks, located below the Curie transition in Fig. 6, are relaxation peaks [21, 22, 29]. The first peak occurred around 183°C for both specimens is independent on composition, while the second relaxation peak is observed at 268°C and 242°C for x=0.05 and 0.2, respectively, i.e., the peak temperature is decreased with the increase of Sr content. Applying the Arrhenius relaxation equation and using the previous results of Ref. [29], it is found that the calculated activation energy for the first peak is 1.248 eV. Since this value is greater than 1.1 eV, the first peak could be attributed to diffusion of point defects in ferroelectric phase [38] of tested BST ceramics. On the other hand, the calculated values of activation energy corresponding to the second relaxation peaks are 0.928 and 0.998 eV for x=0.05 and 0.2, respectively. Therefore, the origin of these peaks could be attributed to the diffusion of oxygen vacancies associated with domain walls in these polycrystalline ceramics [22, 29].

5 Conclusion

$Ba_{1-x}Sr_xTiO_3$ ceramics with x=0.05, 0.1, 0.15 and 0.2 were prepared by solid state reaction technique and were studied by XRD and ultrasonic techniques. XRD data confirmed the formation of single phase perovskite structures. Density, longitudinal velocity, elastic modulus, and attenuation showed composition and sintering time dependence. Increasing of strontium content resulted in a decrease of bulk density and ultrasonic attenuation (at 2 MHz), and an increase in velocity and modulus. The effect of increasing sintering time on BST microstructure revealed an increase in c/a ratio, indicating the decrease of particle size, as confirmed by XRD studies. In spite of ultrasonic velocity and longitudinal modulus were generally increased with Sr content, both showed a nonlinear dependence on sintering time. The temperature dependence of ultrasonic attenuation for x=0.05 and 0.2 revealed, not only, the Curie (C-T) transition and the right shoulder of (T-O) transition, but also two relaxation peaks associated with point defects and oxygen vacancies.

References

1. H.V. Alexandru, C. Berbecaru, A. Ioachim, L. Nedelcu, A. Dutu, Appl. Surf. Sci. **253**, 354 (2006)
2. Z. Wang, S. Jiang, G. Li, M. Xi, T. Li, Ceram. Int. **33**, 1105 (2007)
3. C. Mao, X. Dong, T. Zeng, H. Chen, F. Cao, Ceram. Int. **34**, 45 (2008)
4. U. Ellerkmann, R. Liedtke, U. Boettger, R. Waser, Appl. Phys. Lett. **25**, 4708 (2004)
5. S. Sreekantan, A. Fauzi, M. Noor, Z.A. Ahmad, R. Othman, A. West, D. Sinclair, J. Mater. Sci. **42**, 2492 (2007)
6. S.K. Rout, S. Panigrahi, J. Bera, Mater. Sci. Eng., B **99**, 8 (2001)
7. S.K. Rout, J. Bera, in *Ferroelectrics and dielectrics*, ed. by A.P. Tandon. (Allied Publishers Pvt. Ltd., New Delhi, 2004), p. 3–7
8. W.F. Hu, D. Zhang, M.J. Lancaster, T.W. Button, B. Su, IEEE Trans. Microw. Theor. Tech. **55**, 418 (2007)
9. B. Su, J.E. Holmes, C. Meggs, T.W. Button, J. Eur, Ceram. Soc. **23**, 2699 (2003)
10. N. Setter, R. Waser, Acta Mater. **48**, 151 (2000)
11. P.P. Phule, S.H. Risbud, J. Mater. Sci. **25**, 2571 (1990)
12. X. Yang, X. Yao, L. Zhang, Ceram. Int. **30**, 1525 (2004)
13. X. Wei, N. Padture, Ceram. Process. Res. **5**, 175 (2004)
14. B. Gresten, M. Lencka, R. Riman, J. Am. Ceram. Soc. **87**, 2025 (2004)

15. H. Reveron, C. Elissald, C. Aymonier, C. Bousquet, M. Maglione, F. Cansell, Nanotechnology **17**, 3527 (2006)
16. J. Liu, Z.J. Shen, M. Nygren, B. Su, T.W. Button, J. Am. Ceram. Soc. **89**, 2689 (2006)
17. T. Hungria, M. Alguero, A. Hungria, A. Castro, Chem. Mater. **17**, 6205 (2005)
18. L. Zhou, P.M. Vilarinko, J.L. Baptista, J. Eur. Ceram. Soc. **21**, 531 (2001)
19. H. Guo, J. Cannata, K.K. Shung, J. Mater. Sci. **40**, 1509 (2005)
20. L. Szymczak, Z. Ujma, J. Handerek, J. Kapusta, Ceram. Int. **30**, 1003 (2004)
21. B.L. Cheng, M. Gabbay, G. Fantozzi, W. Duffy Jr., J. Alloy. Comp. **211**, 352 (1994)
22. B.L. Cheng, M. Gabbay, M. Maglione, G. Fantozzi, J. Electroceram. **10**, 5 (2003)
23. H.V. Alexandru, C. Berbecaru, A. Ioachim, Mater. Sci. Eng., B **109**, 152 (2004)
24. E.A. Parker, S.B. Savia, IEE Proc. Microwaves Antenn. Propag. **148**, 103 (2001)
25. M.F. Iskander, Z.Q. Yun, Z.J. Zhang, et al., Asia-Pacific Microwave Conf., Sydney, Australia, 814 (2000)
26. E.C. Subbarao, G. Shirane, J. Am. Ceram. Soc. **42**, 279 (1959)
27. H.V. Alexandru, C. Berbecaru, F. Stanculescu et al., Mater. Sci. Eng. **B118**, 92 (2005)
28. C. Fu, C. Yang, H. Chan, Y. Wang, L. Hu, Mater. Sci. Eng. **B 119**, 185 (2005)
29. H. Frayssignes, B.L. Cheng, G. Fantozzi, T.W. Button, J. Eur. Ceram. Soc. **25**, 3203 (2005)
30. V. Rajendran, J. Non-Cryst. Solids **353**, 77 (2007)
31. A. Ioachim, M.I. Toaxan, M.G. Banclu, L. Nedelcu, A. Dutu, S. Antohe, C. Berbecaru, L. Georescu, G. Stoica, H.V. Alexandru, Thin Solid Films **515**, 6289 (2007)
32. C. Berbecaru, H.V. Alexandru, C. Porosnicu, A. Vele, A. Ioachim, L. Nedelcu, M. Toascan, Thin Solid Films **516**, 8210 (2008)
33. Y.C. Liou, C.T. Wu, Cerm. Int. **34**, 517 (2008)
34. S. Kongtaweelert, D.C. Sinclair, S. Panichphant, Curr. Appl. Phys. **6**, 474 (2006)
35. A.K. Singh, S.K. Barik, R.N.P. Choudhary, P.K. Mahapatara, J. Alloy. Compd. **479**, 39 (2009)
36. I. Malecki, J. Ranachowski, Physical Foundation of Ultrasonic Research Trends and its Application in Poland, Warsaw, Poland (1981)
37. B.L. Cheng, B. Su, J.E. Holmes, T.W. Button, M. Gabbay, G. Fantozzi, J. Electroceram. **9**, 17 (2002)
38. V.S. Postnikov, V.S. Pavlov, S.A. Gridnev, S.K. Turkov, Sov. Phys. Solid State **10**, 1267 (1968)
39. H. Abdelkefi, H. Khemakhem, G. Velu, J.C. Carru, R. Von der Muhll, J. Alloy. Compd. **399**, 1 (2005)